nature communications

Article

https://doi.org/10.1038/s41467-025-59944-3

# Bioinspired learning and memory in ionogels through fast response and slow relaxation dynamics of ions

Received: 4 December 2024

Accepted: 9 May 2025

Published online: 16 May 2025

Check for updates

Ning Zhou, Ting Cui, Zhouyue Lei ✉ & Peiyi Wu ✉

Mimicking biological systems' sensing, learning, and memory capabilities in synthetic soft materials remains challenging. While significant progress has been made in sensory functions in ionogels, their learning and memory capabilities still lag behind biological systems. Here, we introduce cation-π interactions and a self-adaptable ionic-double-layer interface in bilayer ionogels to control ion transport. Fast ion response enables sensing and learning, while slow ion relaxation supports long-term memory. The ionogels achieve bioinspired functions, including sensitization, habituation, classical conditioning, and multimodal memory, with low energy consumption (0.06 pJ per spike). Additionally, the ionogels exhibit mechanical adaptability, such as stretchability, self-healing, and reconfigurability, making them ideal for soft robotics. Notably, the ionogels enable a robotic arm to mimic the selective capture behavior of a Venus flytrap. This work bridges the gap between biological intelligence and artificial systems, offering promising applications in bioinspired, energy-efficient sensing, learning, and memory.

Biological intelligence arises from the seamless integration of rapid sensing, associative learning, and long-term memory, processes fundamentally controlled by the selective transport and dynamic relaxation of ions[1–4]. These ion-regulated mechanisms allow biological systems to respond, adapt, and store information with efficiency. Inspired by these natural processes, synthetic ionic materials such as hydrogels and ionogels have garnered significant attention for their potential to mimic sensory functions. Recent advances have enabled these materials to replicate basic sensory behaviors, demonstrating their utility in bioinspired systems[5–9]. However, their ability to achieve higher-order functions such as learning and memory remains severely limited, falling far short of the capabilities of their biological counterparts. Bridging this gap is critical to advance the development of intelligent soft materials that integrate perception, learning, and memory, offering transformative opportunities in wearable devices, soft robotics, and adaptable systems[10].

To compensate the limitations of soft ionic materials, traditional solid-state semiconductors are used for signal processing and data storage due to their tunable electronic properties, including rectification and non-linear current-voltage characteristics[11]. More recently, semiconductor heterostructures have also been combined with ionic interfacial layers to enable environmental sensing and signal processing within these hybrid devices[12,13]. While these approaches achieve high efficiency, they fundamentally rely on the charge injection and storage properties of inorganic semiconductors, rather than fully utilizing the intrinsic capabilities of the ionic materials. The reliance on solid-state components inherently lacks the flexibility, stretchability, and self-healing properties that are features of biological tissues, ultimately restricting their mechanical compatibility and adaptability for real-time interaction with soft biological and ionic systems[9]. In the search for more biologically compatible solutions, people have explored polyelectrolyte fluids within confined micro- or nanochannels to develop fluidic ionic diodes, transistors, and memristors[2,14,15]. While promising, these approaches are often hampered by stability issues, particularly the risk of leakage associated with aqueous media[16]. Quasi-solid ionogels offer an alternative, as they can mitigate leakage while translating external stimuli into changes in ion distribution, enabling the stimulus sensing and signal rectification

State Key Laboratory of Advanced Fiber Materials, College of Chemistry and Chemical Engineering, Center for Advanced Low-Dimension Materials, Donghua University, Shanghai, China. ✉e-mail: leizhouyue@dhu.edu.cn; wupeiyi@dhu.edu.cn

observed in biological systems[5,7,17–20]. However, existing ionogels still face a challenging trade-off between fast response and slow relaxation dynamics of ions, which is critical to achieving high sensitivity, associative learning, and long-term memory functionalities in a unified framework[21,22].

Herein, we present a non-volatile bilayer ionogel that exploits cation-π interactions and a self-adaptable ionic-double-layer (IDL) interface to achieve both fast response and slow relaxation dynamics of ions. Cation-π interactions within the ionogel selectively bind cations, facilitating fast response and transport of free anions. While the IDL promotes ion accumulation at the interface, providing the basis for slow relaxation dynamics of bound ions. This design enables the ionogel to perform associative learning and bioinspired memory functions, significantly enhancing the intelligence of conventional soft ionic materials. In addition, both of the two layers in the ionogel exhibit mechanical adaptability, with physically cross-linked networks that allow them to be reconfigured and reshaped like "Lego blocks". This work paves the way for the development of a generation of soft materials capable of dynamic sensing, learning, and memory.

## Results

### Bioinspired design of self-adaptable IDL

In biological sensory nervous systems, interaction-gated ion channels within cell membranes control selective ion transport and distribution, facilitating ionic signal selectivity, adaptation, and gain modulation. For instance, neurotransmitters such as acetylcholine utilize cation-π interactions to bind with their receptors, triggering selective ion transport that induces synaptic depolarization or hyperpolarization, thereby modulating postsynaptic neuronal excitability (Fig. 1a)[23]. Here, we design ionogels with the bioinspired cation-π interaction to modulate ion distribution and relaxation dynamics (Fig. 1a and Supplementary Fig. 1). A hydrophobic and environmentally stable $[EMIM]^+$ $[TFSI]^-$ ionic liquid is selected as the primary ionic carrier. The ionogels are composed of a cationic polyacrylate block (CPB) and a neutral polyacrylate block (NPB), thus forming a Janus interface. In the NPB, oligo(ethylene glycol) methyl ether acrylate (OEGA) and methyl acrylate (MA) are used to fabricate a polymer matrix with soft chain segments. In the CPB, benzyl acrylate (BzA) monomers engage in cation-π interactions with the cations from the comonomers ($[DMAEA\text{-}Q]^+$

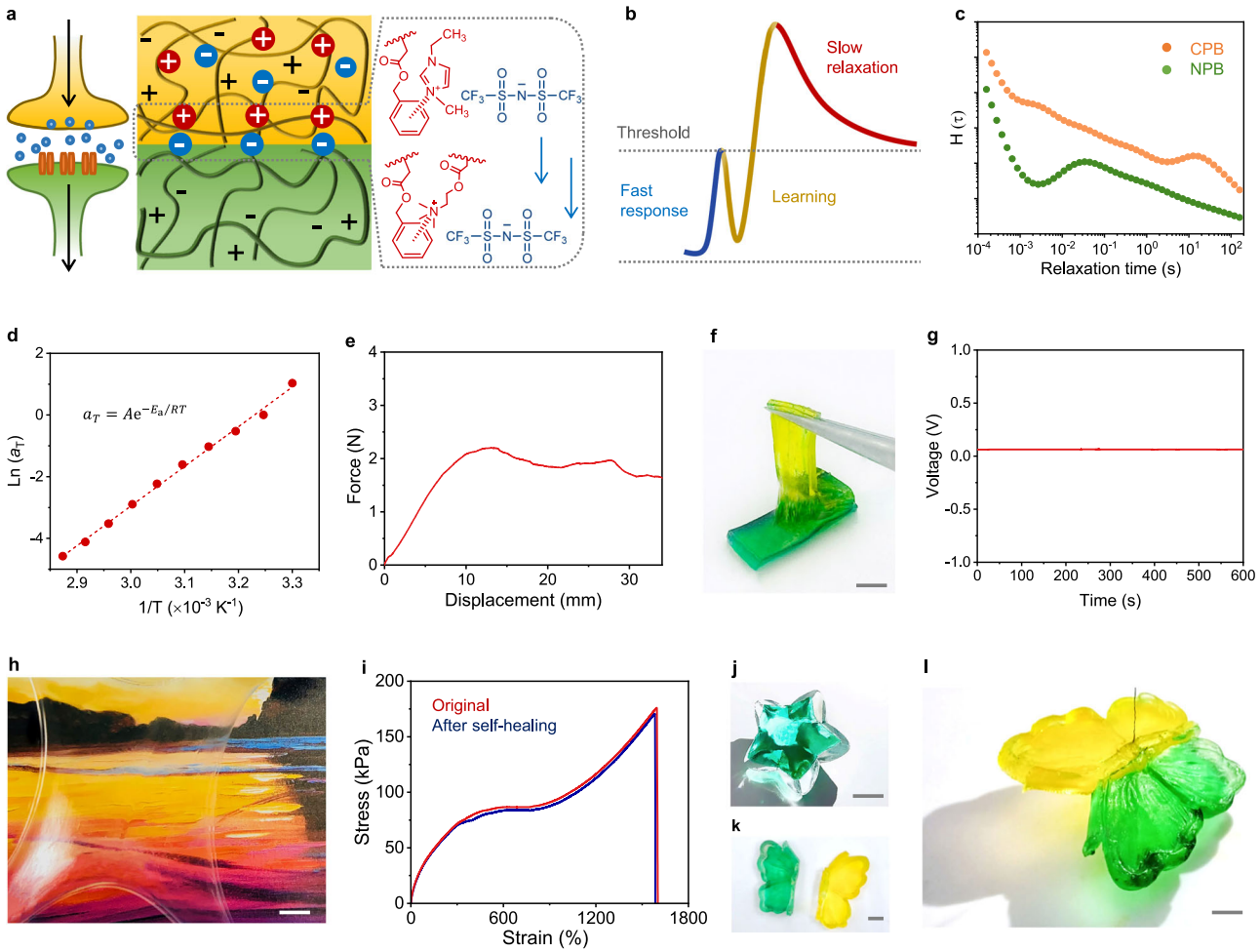


**Fig. 1 | The design of the bilayer ionogel. a** Schematic illustration of neurotransmitter modulation of postsynaptic nerve excitability and self-adaptable IDL modulation of the ion transports in ionogels. The yellow square indicates CPB and the green square indicates NPB. Schematic lines are used to represent the internal polymer chains. Red spheres represent positively charged cations, and blue spheres represent negatively charged anions. **b** Schematic description of fast response and slow relaxation characteristics of the bilayer ionogel. **c** Relaxation time spectra of CPB (orange) and NPB (green). **d** Time-temperature superposition shifts at a reference temperature of 25 °C. **e** The 180° peeling force-displacement curve of the CPB and NPB. **f** The finger-like patterns at the Janus interface. The CPB is dyed yellow and the NPB green. Scale bar: 10 mm. **g** Open-circuit voltage of the bilayer ionogel. **h** A photo of the transparent and stretchable bilayer ionogel composed of CPB and NPB. Scale bar: 10 mm. **i** The stretching curves before (red) and after (blue) the self-healing of the bilayer ionogel. **j** The bilayer ionogel demonstrating exceptional mechanical adaptability by conforming to an irregular pentagonal plastic surface. The ionogel is dyed green for better visualization. Scale bar: 5 mm. **k** A photo of the bilayer ionogel is prepared in a butterfly-shaped mold, in which CPB and NPB are dyed yellow and green, respectively. Scale bar: 5 mm. **l** A photo of the self-healing bilayer ionogel. Scale bar: 5 mm.

$[TFSI]^-$) and the ionic liquid ($[EMIM]^+$ $[TFSI]^-$) (Supplementary Fig. 2). When the two ionogels (CPB and NPB) are combined, an IDL forms at the interface of the bilayer ionogels. Upon stimulation, the bilayer ionogels achieve rapid electrical signal responses through the fast transport of free anions and require only a short learning time to reach the set threshold (Fig. 1b). After the response, the slow relaxation of the ions within the bilayer ionogel allows long-term memory to be maintained.

The cation-π interactions are quantitatively analyzed by isothermal titration calorimetry (ITC)[24,25]. When mixed $[EMIM]^+$ $[TFSI]^-$ and $[DMAEA\text{-}Q]^+$ $[TFSI]^-$ are titrated with BzA, the cation-π interactions result in an exothermic enthalpy ($\Delta H = -1.9$ kJ mol$^{-1}$, Supplementary Note 1 and Supplementary Fig. 3). Moreover, the binding of BzA units to $[DMAEA\text{-}Q]^+$ and $[EMIM]^+$ cations leads to increased dissociation of anions from their counterions, as evidenced by the elevated entropy ($\Delta S = 31.8$ J mol K$^{-1}$). On the one hand, these high-entropy anions tend to diffuse towards the NPB side. On the other hand, they are attracted by the excess cations in the CPB. Consequently, the presence of strong cation-π interactions propels the anions to accumulate at the Janus interface of CPB and NPB and form an IDL (Supplementary Note 2). To confirm the existence of the IDL, AC-impedance measurements are conducted, and the data are analyzed by an equivalent circuit model[18,19]. The IDL capacitance ($C_{IDL}$) values of the CPB/CPB and NPB/NPB homojunctions are about 1.31 μF cm$^{-2}$ and 0.29 μF cm$^{-2}$, respectively, while the CPB/NPB heterojunction exhibits a significantly lower capacitance of only 0.02 μF cm$^{-2}$ (Supplementary Fig. 4, Supplementary Note 3, and Supplementary Table 1). This difference indicates the presence of a low-capacitance planar IDL at the CPB/NPB interface[18]. Furthermore, when a reverse bias of −1 V is applied, mobile ions accumulate at the interface, disrupting the IDL and resulting in a decrease in interfacial resistance. This disruption leads to a reduction in low-frequency (<100 Hz) impedance (Supplementary Fig. 5). In contrast, applying a forward bias of +0.35 V strengthens the IDL, which increases the low-frequency impedance. These observations are consistent with previous studies on IDL behavior and provide strong evidence for the existence of the IDL at the CPB/NPB interface[18,19].

The physically cross-linked networks in the CPB exhibit two distinct relaxation modes: slow relaxation at 13 s and ultrafast relaxation at 0.003 s (Fig. 1c)[26]. As ion transport is governed by the relaxation modes of polymer segments, the transport rates of the $[EMIM]^+$ cation and $[TFSI]^-$ anion in CPB are linked to the slow and ultrafast segmental relaxations, respectively[27,28]. In contrast, the NPB exhibits a single relaxation peak at 0.03 s, associated with the relaxation time of neutral polyacrylate segments. Consequently, the transport rates of both cations and anions in NPB are similar, slower than the anion transport rate in CPB but faster than its cation transport rate. Additionally, the strong cation-π interactions in CPB attract $[TFSI]^-$ anions from NPB, accumulating at the Janus interface. This ionic distribution further stabilizes the slow diffusion of $[TFSI]^-$ in NPB, providing the tunable relaxation dynamics of the ions. The thermodynamic model of the IDL is further summarized in Supplementary Note 4.

Finite element modeling (FEM) is employed to reveal the ion distribution under different electric fields (Supplementary Fig. 6 and Supplementary Note 5)[14,18]. Upon the stimuli of an external electric field, the ions especially the $[TFSI]^-$ anions are away from the equilibrium state. When an electric field capable of eliminating the IDL is applied, it induces a high current in the ionogel. Conversely, an opposite electric field which strengthens the IDL, leads to a relatively small current due to the depletion of mobile ions in the IDL. After the removal of the external electric field, the spontaneous movements of $[TFSI]^-$ anions are driven by entropy and the restoration of IDL.

The cation-π interactions and polymer entanglement contribute to physical crosslinking in the ionogels. The time-temperature superposition analysis reveals an apparent activation energy ($E_a$) of ~107 kJ mol$^{-1}$ for the physically cross-linked networks in the ionogels (Fig. 1d, Supplementary Fig. 7, and Note 6)[29]. Moreover, the internal electric field of the IDL provides electrostatic force and self-adhesion between CPB and NPB with an interfacial toughness exceeding 439 J m$^{-2}$ in 180-degree peel tests (Fig. 1e). As the peeling force increases, the presence of finger-like patterns before the interfacial crack propagation further demonstrates the tough bonding of the Janus interface (Fig. 1f). In the absence of BzA, the bilayer ionogels exhibit significantly lower interfacial toughness of only 179 J m$^{-2}$ (Supplementary Fig. 8). It indicates that the cation-π interactions induced by BzA enhance the interfacial adhesion between CPB and NPB. Moreover, the IDL demonstrates tunable interfacial adhesion upon the application of a bias voltage (Supplementary Fig. 9)[30]. When a forward bias is applied, the IDL is reinforced, leading to an increase in interfacial adhesion. In contrast, applying a reverse bias disrupts the IDL, thereby weakening the adhesion. While the same electric fields applied to the NPB/NPB homojunction result in minimal changes in adhesion. These electrostatic adhesion behaviors observed in peel tests further confirm the formation of the IDL at the CPB/NPB interface and its ability to be modulated by the applied bias.

Under resting conditions, mobile ions are located at an equilibrium state and depleted in the IDL. The internal electric field within the IDL directs from the CPB to the NPB. The open-circuit voltage of the ionogels is ~63 mV (Fig. 1g), which closely aligns with the resting potential of neural cell membranes (~70 mV). However, in the bilayer ionogels without BzA, there is no cation-π interaction to selectively bind cations or facilitate the transport of free anions. As a result, the open-circuit potential of the bilayer ionogels without BzA is significantly reduced, measuring only around 43 mV (Supplementary Fig. 10).

The bilayer ionogels display high transparency and stretchability (Fig. 1h). CPB and NPB exhibit different moduli and elongations at break (Supplementary Fig. 11). When combined to form a bilayer ionogel, the strong interfacial adhesion provided by the IDL enables the two layers to sustain deformation in tandem. The nearly horizontal plateau observed in the strain range of 500%–800% can be attributed to the influence of the NPB (Fig. 1i). At the strain around 600%, the NPB begins to develop defects due to its lower modulus and mechanical limits compared to CPB. However, thanks to the strong interfacial adhesion with the CPB via the IDL, the NPB remains partially intact and does not fully delaminate or separate from the CPB surface. Therefore, the bilayer ionogels experience negligible stress mismatch within the strain range of 0–600%. The bilayer ionogels show a Young's modulus of about 100 kPa, which is mechanically comparable to many biological tissues. The maximum elongation-at-break reaches 1603%. They exhibit perfect mechanical adaptability on irregular surfaces, maintaining strong bonding between the CPB and NPB (Fig. 1j). Even with a notch, the ionogels can be stretched to a strain of about 1320% (Supplementary Fig. 12). The toughness is calculated to be about 1850 J m$^{-2}$, comparable to that of biological cartilages (Supplementary Note 7)[31,32].

The ionogels also exhibit self-healing capabilities and reconfigurability. A notch in the material autonomously self-heals at room temperature within 12 h (Supplementary Fig. 13). When the ionogels are cut into two halves, their self-healing efficiency reaches 99% within 12 h at room temperature (Fig. 1i, k, l, Supplementary Note 8). Meanwhile, the open-circuit voltage recovers to 101.6% of its initial state, indicating successful self-healing (Supplementary Fig. 14). Besides, when subjected to cyclic shear strains ranging from 1000% to 0.1%, the storage modulus and loss modulus of the bilayer ionogels rapidly recover at small strains (Supplementary Fig. 15). The bilayer ionogels can be easily assembled into various shapes (Supplementary Fig. 16). These properties arise from the viscoelastic nature of the bilayer ionogels and further highlight their reconfigurability, similar to assembling "Lego blocks" without compromising their functional or mechanical integrity. It is distinct from, but complementary to, the

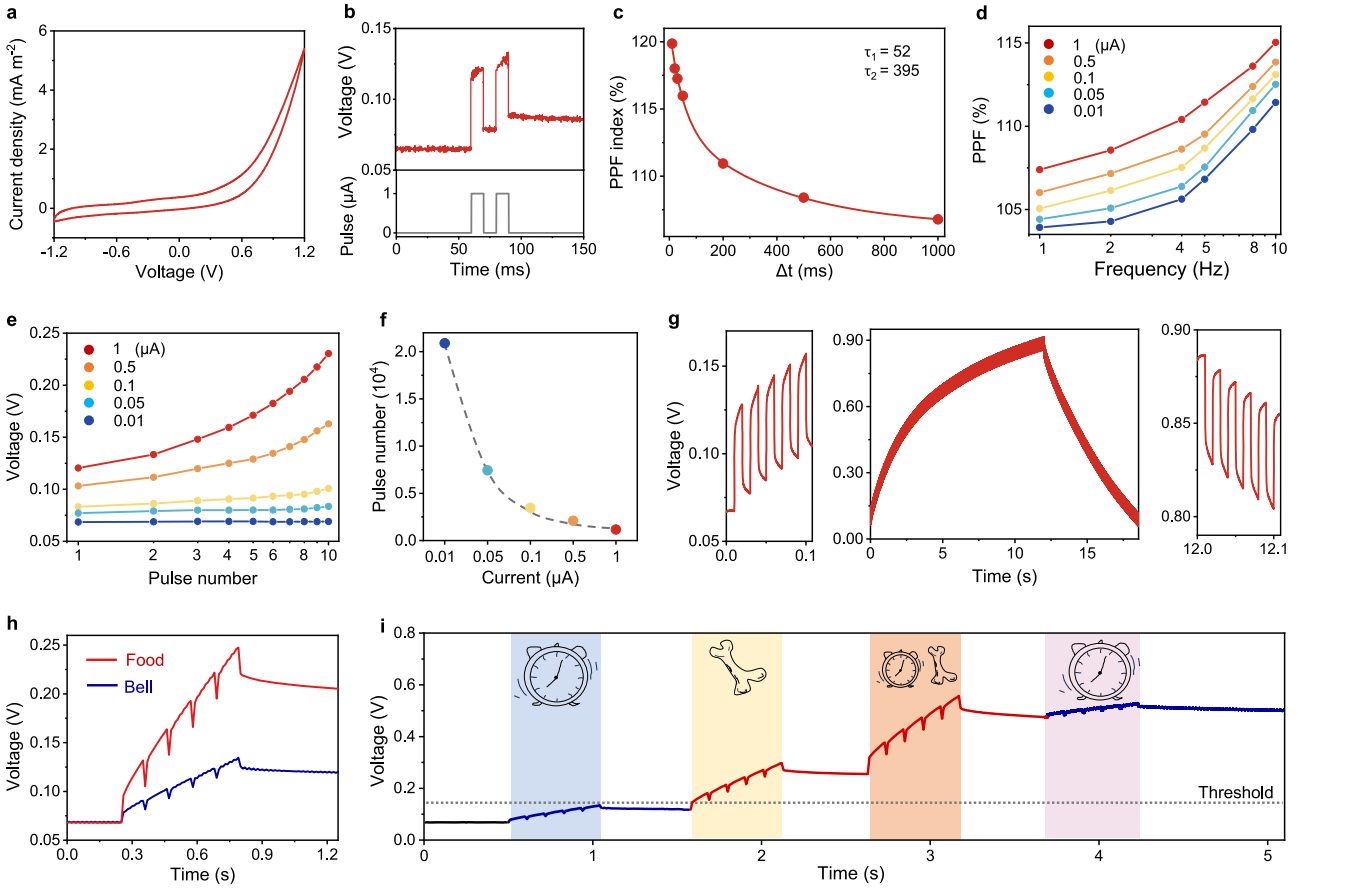


**Fig. 2 | Biological associative learning of the bilayer ionogel. a** The *I–V* curve of the bilayer ionogel (scan rate: 1 mV s$^{-1}$). **b** The voltage response of the bilayer ionogel upon being triggered by paired pulses with the Δ*t* of 10 ms. **c** An exponential fitting curve showing the PPF behavior and characteristic timescales of the bilayer ionogel. **d** The PPF behavior of the bilayer ionogel triggered by different currents at 1 (red), 0.5 (orange), 0.1 (yellow), 0.05 (blue), 0.01 (deep blue) μA and frequencies. **e** Voltage response of the bilayer ionogel triggered by different currents at 1 (red), 0.5 (orange), 0.1 (yellow), 0.05 (blue), 0.01 (deep blue) μA and pulse numbers. **f** The number of pulses required to saturate the response voltage of the bilayer ionogel under different pulse currents at 1 (red), 0.5 (orange), 0.1 (yellow), 0.05 (blue), 0.01 (deep blue) μA. **g** Voltage response of the bilayer ionogel under forward and backward current pulses. **h** Voltage response of the bilayer ionogel by applying a food (red) pulse of 0.8 μA and a bell (blue) pulse of 0.2 μA. **i** The bilayer ionogel exhibits a voltage response exceeding the "salivation" threshold in response to bell stimuli after undergoing conditional learning. Sketches of a bell and food represent different stimuli. The red curve represents the food or bell +food stimulus, while the blue curve represents the bell stimulus alone.

gel's self-repair capability. Importantly, unlike hydrogels that lose water and shrink in open air after 48 h, the ionogels incorporated with the $[EMIM]^+$ $[TFSI]^-$ ionic liquid maintain their original shapes and demonstrate environmental stability (Supplementary Fig. 17).

## Bioinspired associative learning

The electrical self-adaptability of the IDL imparts the ionogels with asymmetric and non-linear rectification effects for ion flows (Supplementary Note 9)[33]. The current density in the "on" state of the bilayer ionogels with BzA is significantly higher than that of the structure without BzA (Fig. 2a and Supplementary Fig. 18). However, an excessive amount of the BzA monomer leads to a decreased current density due to the increased mechanical stiffness of the polymer networks, which limits the ion mobility and the rectification effect[24]. The optimal molar ratio of the $[DMAEA\text{-}Q]^+$ $[TFSI]^-$, BzA, and OEGA is 3.4:2:1. The maximum rectification ratio reaches about 11 at a scan rate of 1 mV s$^{-1}$, which is higher than that of some hydrogel ionotronics (Fig. 2a)[34]. The hysteresis loop area of the *I–V* curve increases with the scan rate, indicating that there are slow ion relaxation dynamics and non-faradaic behaviors (Supplementary Fig. 19)[34]. In addition, the ionogels have a wider electrochemical window (−2 to 2 V) compared to hydrogels (usually in the range of −1.2 to 1.2 V) because they avoid redox reactions from water splitting (Supplementary Fig. 20).

When paired electrical stimuli are applied to the bilayer ionogel, they induce a voltage increase (ΔV) at the second stimulus, analogous to the paired-pulse facilitation (PPF) observed in the short-term plasticity (STP) of biological sensory neuron systems (Fig. 2b)[35]. The PPF index of the ionogels is defined as $A_2/A_1 \times 100\%$, where $A_1$ and $A_2$ are the amplitudes of the first and the second response voltage, respectively[36]. The bioinspired PPF behavior may be attributed to the first stimulus strengthening the IDL and dissociating more ions from cation-π and ionic interactions (Supplementary Note 10). During the intervals between pulse stimuli, the relatively slow relaxation mode of $[TFSI]^-$ anions on the NPB side helps partially maintain the strengthened IDL state. This dynamic sets the stage for the second stimulus, effectively encoding the memory of the first stimulus and enhancing the amplitude of the second response. The ΔV and PPF increase as the time interval (Δ*t*) decreases, and vice versa. This behavior demonstrates the ability of the ionogels to mimic the modulation of the synaptic weight (i.e., the strength of a synapse) observed in biological STP (Fig. 2c and Supplementary Fig. 21). Upon a paired electrical stimulus of 1 μA, the characteristic timescales ($\tau_1$ and $\tau_2$), fitted by an exponential curve, are determined to be 52 and 395 ms, respectively. These timescales are comparable to those of neuron activities in the human brain, which are on the order of milliseconds. Furthermore, the PPF behavior of the ionogels is observed across a broad range of

stimulus (pulse) strengths (Fig. 2d and Supplementary Figs. 22–26). Moreover, there is a slight increase from 111% to 115% when the stimulus current is raised from 0.01 to 1 μA (at 10 Hz), likely because higher-strength stimuli exert more influence on ion enrichment and IDL state. Besides, stimulation at higher frequencies allows the ions to reach the saturation state more quickly, resulting in a smaller increase in the amplitude of the voltage. Importantly, even fractured ionogels can fully recover the PPF behavior after self-healing, highlighting the robustness and reliability of the bilayer ionogel (Supplementary Fig. 27).

For subsequent stimuli, the IDL and external electric field jointly determine the short-term distribution of the ions during the pulse interval. This behavior closely resembles sensitization, which is an elementary form of biological associative learning (Supplementary Note 11). As the number of pulses increases, the response voltage continues to rise (Fig. 2e and Supplementary Fig. 28). After receiving ten consecutive stimuli at 1 μA, the response voltage reaches ~0.23 V. On the other hand, the ionogels exhibit different plateau voltages in response to stimuli of varying strengths and pulse numbers (Fig. 2f and Supplementary Fig. 28). Compared to larger pulse stimuli, smaller pulse stimuli generate lower plateau voltages. Moreover, weaker stimuli require a greater number of pulses to reach the plateau state. This behavior is because the IDL and enriched ions at the ionogel-electrode interface approach saturation as the stimulus strength and pulse number reach a threshold. The presence of cation-π interactions and the IDL stabilizes the ion-enriched state, resulting in even slower relaxation dynamics under saturation, which enhances the voltage memory. Consequently, the ΔV between neighboring stimuli gradually diminishes to zero, indicating the adaptation of the ionogels to external stimuli, similar to habituation which is also an elementary form of biological associative learning.

The energy consumption ($W$) of the ionogels is further calculated based on the integration of the $V$–$t$ response curves under single pulses[37]. The $W$ is determined by the integration over the pulse width, which is also related to the size of the ionogels (Supplementary Fig. 29a). For the bilayer ionogels with an area of 150 $mm^2$, $W$ is only 0.06 pJ per spike (Supplementary Fig. 29b). The ultra-low energy consumption is close to the biological energy consumption and even an order of magnitude lower than that of a previously reported fluidic memristor[14,38].

When subjected to a series of 100 pulses, the bilayer ionogel can achieve 100 distinct states, enabling an information writing process (Fig. 2g). By injecting a forward pulse, the ionogel exhibits different ionic signals, effectively representing information. Conversely, backward stimuli can erase this information. The writing-erasing state can be programmed by varying the number or amplitude of the stimuli pulse (Supplementary Fig. 30). For stimuli of the same frequency (50 Hz) and duration (10 ms), lower amplitude current stimuli result in smaller incremental voltage changes, allowing for the generation of multiple distinct writing states.

In addition to sensitization and habituation, classical conditioning as another fundamental form of associative learning in biological systems[39], can also be emulated by implementing dual inputs on the bilayer ionogel. Here, we mimic classical Pavlovian conditioning by applying a food pulse of 0.8 μA and a bell pulse of 0.2 μA. The threshold for the "salivation" response is set at 146 mV. After five consecutive food stimuli, the voltage response reaches 247 mV, significantly higher than the salivation threshold and the response observed with the five bell stimuli, which is only 135 mV (Fig. 2h). However, after conditional learning, the ionogels can generate a robust response of 552 mV solely to the bell pulse, surpassing the threshold and eliciting a salivation response (Fig. 2i). This learning behavior is due to the cumulative effect of slow ion relaxation following each stimulus. The slow relaxation preserves the effects of previous stimuli, enabling the ionogels to retain a persistent memory of past learning experiences.

## Temporal effects on associative learning behaviors

The ability to encode and process information based on precise temporal sequences and intervals is a fundamental aspect of associative learning in biological systems. By studying the temporal dynamics and modulating the ion distribution of the bilayer ionogel, we provide insights into the design principles for developing quasi-solid ionic systems that can imitate and harness the temporal aspects of associative learning. When two individual stimuli each composed of five spike trainings are applied, the responses depend on the spike strength and number (Fig. 3a, b). Notably, when the two stimuli arrive successively, the ionogels demonstrate the capability to recognize distinct temporal sequencing and time intervals ($\Delta t$), yielding different response patterns. Following the first stimulus of high spike strength, the second stimulus with low spike strength leads to an enhanced response of 190 mV, surpassing the response toward a single stimulus of low spike strength (96 mV). Moreover, exchanging the temporal sequences of the two stimuli also results in different responses. This behavior is likely due to ion accumulation and the slow diffusion relaxation mode induced by the enhancement of the IDL from the first stimulus, which further amplifies the electrical response to the second stimulus. As the time interval between the two stimuli is reduced to 0.1 s, the history-dependent plasticity becomes more evident. The response to the second high-strength stimulus increases to 262 mV. Furthermore, the superposition of the two stimuli generates the highest response, reaching up to 376 mV. The characteristics of spike training can be further analyzed using time-averaging techniques commonly employed in neuroscience, wherein $\Delta t$ and mean firing rates are correlated with synaptic responses (Supplementary Fig. 31 and Supplementary Note 12)[40]. These findings shed light on the capacity of ionogels to imitate the temporal aspects of associative learning and provide a foundation for the development of advanced neuromorphic computing systems.

When stimuli consisting of different frequencies of positive spike training are applied, the response voltage increases with increasing frequency (Fig. 3c). As a result, the bilayer ionogel demonstrates history-dependent as well as spike-rate-dependent behavior, enabling the emulation of the Bienenstock–Cooper–Munro (BCM) rule observed in neural activities. Here, we apply four sets of spike training to the ionogels (Fig. 3d). Each set contains five positive spikes with the same amplitude of 1 μA but different frequencies, 50, 5, 2, and 50 Hz, in sequence. The initial spike training elevates the response level, leading to even higher response voltages for the second and third spike trainings. Although the fourth spike training has the same frequency and strength as the first train, it generates an enhanced response because of the influence of the previous training. Furthermore, we introduce an additional application of negative spike training (the amplitude of each is 0.6 μA and the frequency of each is 50 Hz), which has an inhibitory effect, after each of the positive spike trainings. This rapid reduction in the response voltage suppresses the BCM effect (Fig. 3e). Consequently, the associative learning behaviors of the ionogels can be tuned through both strengthening and resetting, providing a means to modulate the responsiveness of quasi-solid ionogels in an event-based manner.

When four positive spike trainings and one negative spike training are applied to the bilayer ionogel, different occurrence orders of the negative spike lead to distinct memory curves (Fig. 3f). Notably, the occurrence order of the negative spike train significantly affects the decay rate of the ionogels' memory curve (Fig. 3g). To characterize the memory time quantitatively, we employ a modified Kohlrausch equation, which is widely used as a forgetting function in psychology (Fig. 3h and Supplementary Note 13)[14,41]. The later the negative spike training occurs, the faster the memory curve decays, leading to a shorter characteristic memory time ($\tau$). These findings highlight the potential of ionogels for the versatile and adaptable memory function, akin to neural plasticity observed in biological systems.

https://doi.org/10.1038/s41467-025-59944-3

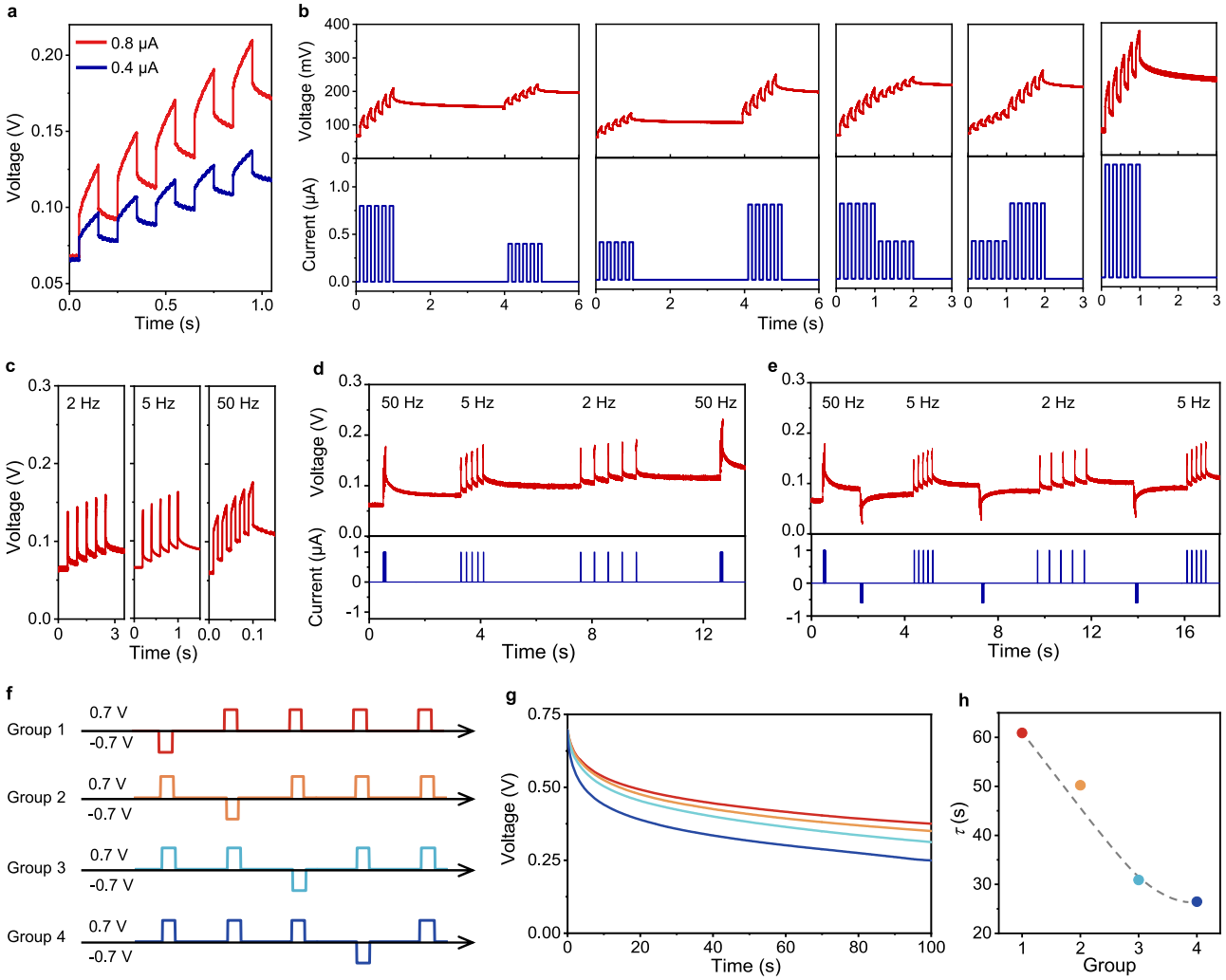


**Fig. 3 | Associative learning behaviors of the bilayer ionogel. a** The voltage response of the bilayer ionogel by applying two different current stimuli (red for 0.8 μA and blue for 0.4 μA). **b** The voltage response of the bilayer ionogel when two different current stimuli arrive in different sequences and time intervals. **c** The voltage response of the bilayer ionogel when the stimuli consisting of different frequencies of positive spike trainings are applied. **d** The voltage response of the bilayer ionogel when a series of positive spike trainings with different frequencies are applied. **e** The voltage response of the bilayer ionogel when a series of positive and negative spike trainings with different frequencies are applied. **f** Four groups of spike trainings (red for Group 1, orange for Group 2, blue for Group 3, and deep blue for Group 4) with different occurrence orders of the negative spike applied to the bilayer ionogel. **g** The voltage memory curves of the bilayer ionogel after four different groups of spike training (red for Group 1, orange for Group 2, blue for Group 3, and deep blue for Group 4). **h** The characteristic memory time of the bilayer ionogel after four different groups of spike training.

## Bioinspired multimodal memory

Memory is a fundamental aspect of biological systems. The transition from sensory memory to short-term memory (STM) and long-term memory (LTM) based on different training numbers and duration time enables the encoding, storage, and retrieval of information (Fig. 4a). In this study, the memory behavior of the bilayer ionogel arises from dynamic changes of the open-circuit voltage (Supplementary Note 14). Upon applying a single 50 s training (10 μA), the bilayer ionogels with BzA retain a voltage of 190 mV after 90 min, maintaining a higher memory strength (about 17%). In contrast, after the same training conditions in the bilayer ionogels without BzA, the memory strength reduces to 0 in only about 33 min (Supplementary Fig. 32). This demonstrates that the inclusion of BzA and the resulting cation-π interaction significantly enhances the memory effect by slowing the ionic relaxation at the interface. For the bilayer ionogels with BzA, its memory voltage remains at 270 mV after 1.5 h when the training duration is increased to 500 s (Fig. 4b). The modified Kohlrausch equation is used to characterize the STM-LTM transition quantitatively. When the training duration increases from 50 to 500 s, $\tau$ increases from 19.3 s to 259 s, indicating the feasibility of the STM-LTM transition in bilayer ionogel (Supplementary Fig. 33)[16]. Even with an equivalent total training duration, memory enhancement can be achieved by employing multiple sets of stimulus training. For example, after 5 sets of 100-s stimulus training, the memory voltage remains at 320 mV even after 1.5 h, exceeding the memory voltage attained after a single 500-s stimulus training (Fig. 4b). This function is similar to the human brain's memory, where repeated learning, as opposed to one-time learning, allows for better memory retention. Furthermore, it takes about 5 days (113 h) for the ionogels to completely forget the training information after the 5 sets of 100-s stimuli (Supplementary Fig. 34). It is anticipated that the memory time of the ionogels can be further extended with an increase in the number or duration of the training sessions. Compared to a prior study using hydrogels for memory effects based on optical signals, the bilayer ionogels exhibit significantly faster electrical signal responses on the millisecond scale, as well as a wider tunable memory retention range, from tens of minutes to several days[22]. Compared to previous reports on polymer gels and elastomers demonstrating rectifying effects, transistor switching

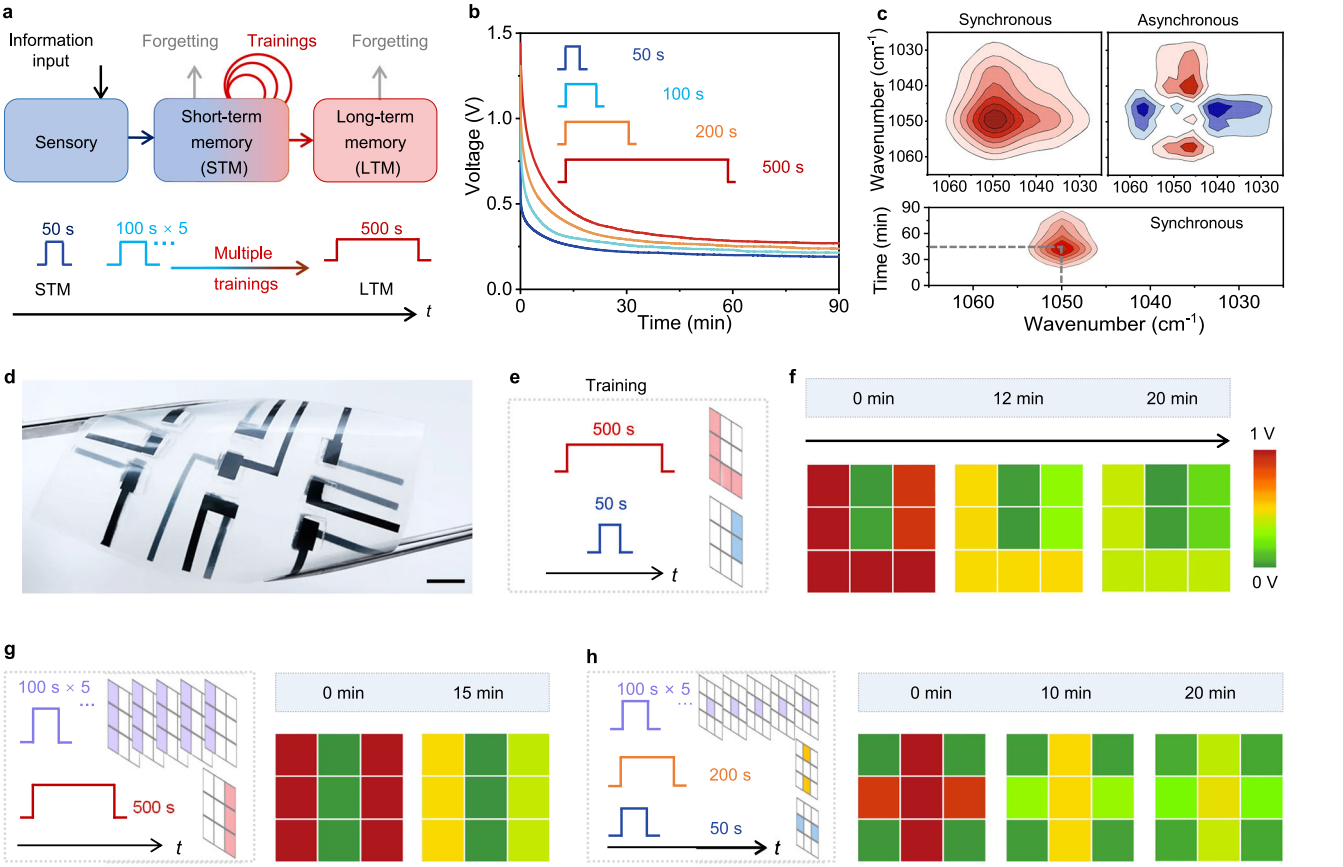


**Fig. 4 | Memory behaviors of the bilayer ionogel. a** The psychological memory model and schematic illustration of training programs for the bilayer ionogel. **b** Memory voltage of the bilayer ionogel after different training programs (red for 500 s, orange for 200 s, blue for 100 s, and deep blue for 50 s). **c** 2D-COS spectra (upper panel) and PCMW spectrum (lower panel) of the bilayer ionogel after 500 s training, red colors represent positive intensities, while blue colors represent negative intensities. **d** A photo of the 3 × 3 array of the transparent bilayer ionogel. Scale bar: 10 mm. **e** Images of the uppercase letter "L" and the number "1" are memorized into the 3 × 3 array by inputting "L" for 500 s and "1" for 50 s. **f** The image of the letter "L" is stored in LTM mode and the number "1" is stored in STM mode. The transition from red to yellow to green represents varying levels of memory intensity. **g** Memory comparison of the two numbers "1" which are individually inputted by 5 sets of 100-s stimulus training (left column) and a single 500-s stimulus training (right column). The transition from red to yellow to green represents varying levels of memory intensity. **h** The multimodal memory after three different training programs. The training programs end at the same time. The transition from red to yellow to green represents varying levels of memory intensity.

functionalities, and excitatory postsynaptic currents, the materials with the introduction of cation-π interactions and ionic interactions not only achieve comparable fast response, but also fill a gap in realizing long-term memory effects lasting several days[18,19].

The bioinspired memory of the bilayer ionogel is mainly attributed to the ion diffusion dynamics, which are synergistically modulated by the IDL and the external electric field. After the 500 s of training (10 μA), the anion diffusion is tracked by in-situ attenuated total reflection Fourier transform infrared (ATR-FTIR) spectra at the CPB-electrode interface. In the FTIR spectra, the peak at 1052 $cm^{-1}$ originates from the antisymmetric stretching vibration of S-N-S in $[TFSI]^-$ anion (Supplementary Fig. 35). After the training, the intensity of the characteristic peak at 1052 $cm^{-1}$ continually decreases, indicating a decline in $[TFSI]^-$ anion concentration. The anions gradually diffuse back into the polymer matrix and reassociate with cations. During the memory process, the decrease in $[TFSI]^-$ anion concentration is further analyzed using two-dimensional correlation spectroscopy (2D-COS) and the perturbation correlation moving window (PCMW) technique (Fig. 4c and Supplementary Note 15)[25]. 2D-COS analysis reveals different states of the $[TFSI]^-$ anions after external stimuli, including free and bound states, corresponding to the characteristic peaks at 1056 and 1050 $cm^{-1}$, respectively. The free anions have a fast relaxation mode while the bound anions have a slow relaxation mode. In the dynamic memory process, the free $[TFSI]^-$ anion (located at 1056 $cm^{-1}$) migrates back first, followed by the recovery of the bound $[TFSI]^-$ anions (located at 1050 $cm^{-1}$). In the 2D PCMW spectra, it is further evident that the most significant change in the $[TFSI]^-$ anions occurs at 45 min after the training. This suggests that, at this point, the majority of $[TFSI]^-$ anions return to their initial equilibrium positions. This behavior is consistent with the trends observed in the voltage memory curve and also reveals the ion dynamics underlying the long-term memory capability of the bilayer ionogel.

The mechanical adaptability and bioinspired memory capabilities of the ionogels present exciting prospects for advancing memory devices and systems. Here, we develop a soft array for information storage and encryption. Fabricated through screen printing, the 3 × 3 array comprises individual pixels composed of bilayer ionogel with identical compositions and geometries (Fig. 4d and Supplementary Fig. 36). Distinct memory voltages correspond to varying memory strengths. Employing two training programs of 500 s and 50 s, we temporarily store images of the uppercase letter "L" and the number "1", respectively (Fig. 4e). Importantly, the training programs end at the same time. At the end of the training, both patterns display a deep red color, indicating high memory strength. However, after 12 min, the number "1" shifts to green, while the letter "L" retains an orange color. After 20 min, the number "1" changes to the background green, whereas the yellow letter "L" remains distinguishable (Fig. 4f).

Additionally, multiple reviews of the stimuli lead to enhanced memory retention compared with one-time stimulus training. After 5 sets of 100-s stimulus training, the number "1" exhibits a higher intensity of yellow after 15 min, whereas the number "1" from a single 500-s stimulus training session appears closer to the background green (Fig. 4g). Comparing the patterns resulting from 5 sets of 100-s stimulus training, a single 200-s stimulus training, and a single 50-s stimulus training, the pattern from the 50-s stimulus is the quickest to be forgotten. After 10 min, the patterns from 5 sets of 100-s stimulus training and a single 200-s stimulus training retain their orange color, whereas only the pattern from the 5 sets of 100-s stimulus training remains readable after 20 min (Fig. 4h and Supplementary Movie 1). These results underscore the potential of using bilayer ionogel with multimodal memory as dynamic pixels for information storage and encryption[22,42,43]. The information stored in the LTM mode can be accessed after the STM mode information has been forgotten.

## Integrating information perception, processing, and memory

The bilayer ionogel integrates information sensing and memory functions through a serial connecting design. For instance, when a pair of the bilayer ionogels with microstructures and without microstructure are connected in series, the ionogels with microstructures could serve as pressure-sensing units, modulating the response voltage of the memory ionogels without microstructures. (Fig. 5a and Supplementary Fig. 37). We subsequently construct a 3 × 3 array, where the top and bottom rows represent background pixels, and the middle row depicts each pixel's color, reflecting the voltage intensity of the memory ionogels in the serially connected structure. Three sets of serially connected structures are subjected to the same constant current stimulus (0.1 μA). Without external pressing, the memory ionogel reaches 1.48 V after 200 s because of the ion migration under an external electric field. Pressing the microstructured sensing ionogels generates higher voltage responses in the memory ionogels. (Fig. 5b and Supplementary Note 16).

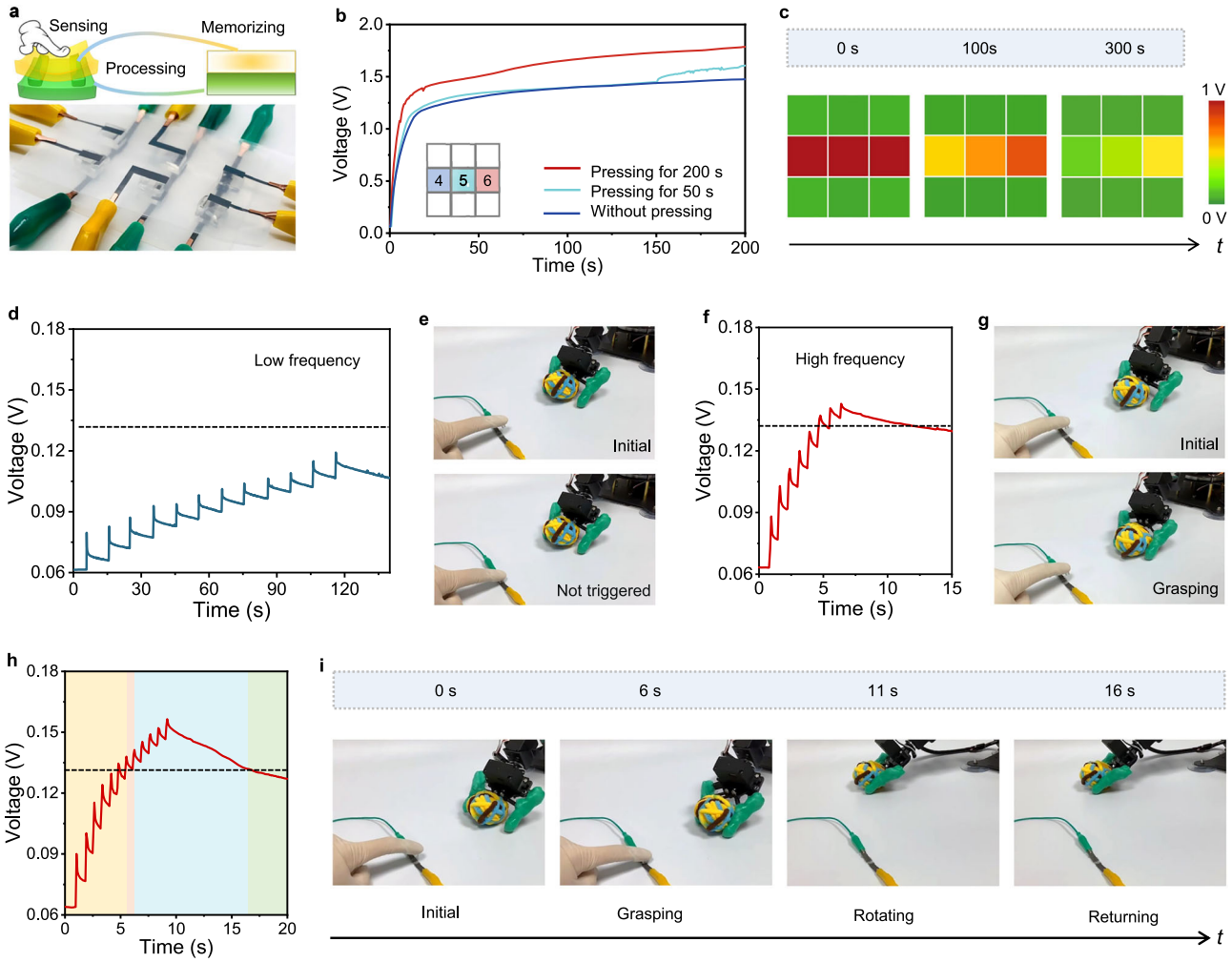


**Fig. 5 | Integrated information sensing, processing, and memory of the bilayer ionogel. a** Schematic illustration and a photo of an ionogel array to demonstrate the information sensing and memory capabilities through a serial connecting of three pairs of the ionogels with microstructures (sensing ionogels) and without microstructures (memory ionogels). The yellow square indicates CPB, and the green square indicates NPB. **b** The voltage response of three different memory ionogels. The three pairs are applied with the same 0.1 μA current stimulus but three different pressing durations (red represents pressing for 200 s, blue represents pressing for 50 s, and purple represents without pressing) are applied on three different sensing ionogels. **c** Three different memory states of the three memory ionogels after their series-connected sensing ionogels experiencing different pressing durations. **d** Voltage response of the memory ionogels when the series-connected sensing ionogels experiencing low-frequency pressing. **e** The photos recording the initial state and still state (after 12 times of low-frequency pressing) of the robotic arm. **f** Voltage response and memory curve of the memory ionogels when the series-connected sensing ionogels experiencing 8 times of high-frequency pressing. **g** Photos recording the initial state and grasping state (after 8 times of high-frequency pressing) of the robotic arm. **h** Voltage sensing ionogels experiencing 12 times of high-frequency pressing. **i** Photos recording the initial, grasping, rotating, and returning states of the robotic arm when the sensing ionogels experiencing 12 times of high-frequency pressing.

At the moment the external electric field is removed, the three middle pixels on the array display a similar deep red color, indicating that all the memory ionogels are in a high-intensity memory state (Fig. 5c). This feature allows for effective encryption of the pressing information. However, after 120 s, the colors of the pixels corresponding to no-pressing or 50-s pressing change significantly, while the pixel corresponding to 200-s pressing retains a deep red color, indicating the LTM effect after the pressing stimulus lasting for 200 s. After 600 s, the left pixel changes to green, indicating the absence of pressing and reading out the no-pressing information. The middle pixel shifts to a light green color, revealing the 50 s pressing information. Only the right pixel remains orange, showing the 200 s pressing information. Therefore, the bilayer ionogel could not only integrate information sensing and memory functions, but also enable information encryption and decryption through the temporal dimension. Importantly, all ionogels (*e.g.*, CPB, NPB, and bilayer ionogels) can withstand 90% compressive strain without breaking (Supplementary Fig. 38). The compression curve of the bilayer structure mainly reflects the compression behavior of NPB at small strains. At large strains, a rapid increase in modulus is observed, similar to the stress enhancement phenomenon in skin under large deformation.

To demonstrate the potential of applying integrated perception, processing, and memory capabilities for developing intelligent robotics, we test the ionogel system using a robotic arm (Supplementary Fig. 39). The movements of the robotic arm are determined by the voltage response of the memory ionogels (Supplementary Note 17). When the sensing ionogels are pressed, the voltage response of the memory ionogels increases. With an increasing number of presses, the voltage of the memory ionogels continues to rise due to the STP effect. This effect is related to the sensitization learning behavior of the ionogels discussed earlier, which enables autonomous processing of the pressing information. However, at a low pressing frequency (0.1 Hz), the relatively long interval between stimulations enables most ions to relax and return to their equilibrium positions. As a result, even after 12 presses on the sensing ionogels, the voltage output of the memory ionogels only reaches 119 mV, which is below the threshold (132 mV) for triggering the movement of the robotic arm (Fig. 5d, e, and Supplementary Movie 2).

In contrast, when the pressing frequency is increased to 1.2 Hz, even with only 8 presses on the sensing ionogel, it could trigger the robotic arm to grasp a woolen ball (Fig. 5f, g, Supplementary Movie 2). With continued high-frequency pressing, the ionic signal of the memory ionogels maintains above the 132 mV threshold for about 1 s, subsequently triggering the robotic arm to rotate (Fig. 5h, i, Supplementary Movie 2). After stopping the pressing, the voltage response of the memory ionogels gradually decreases, falling below the rotation threshold of 140 mV at 14 s, leading to the robotic arm returning to its original position. At 16 s, the voltage drops below the grasping threshold of 132 mV, causing the robotic arm to release the ball. Through the integrated perception, processing, and memory capabilities of the bilayer ionogel, the robotic arm emulates the intelligent response observed in the Venus flytrap. Typically, the Venus flytrap does not react to single, low-frequency stimuli. However, if its sensory hairs are touched multiple times within a short period, the trap rapidly closes. This smart response prevents accidental closure due to nonprey stimuli, such as raindrops. Similarly, the ionogels require continuous high-frequency pressing, which drives the ions to diffuse toward the interface of the bilayer ionogel, progressively approaching the ionic saturation state of the IDL. This process enhances the IDL and promotes slow relaxation of the ions, extending their diffusion time and amplifying the voltage signals. As a result, the ionogels enable the robotic arm to learn and make decisions based on these enhanced signals. The robotic arm effectively avoids unnecessary energy consumption caused by low-frequency interference. In addition, the timing of the robotic arm's return to its original position depends on the duration of the ionogels' memory after the sensitization learning.

## Discussion

In this work, we demonstrate that through rational structural design and modulation of ion transport behaviors, the ionogel can transcend conventional skin-like sensory functions to emulate key biological learning and memory capabilities. By introducing an IDL interface regulated by cation-π interactions, the bilayer ionogel achieves an integration of fast response and slow relaxation dynamics across different ions, enabling bioinspired functions such as sensitization, habituation, classical conditioning, and multimodal memory with an ultra-low energy requirement of only 0.06 pJ per spike. In contrast to rigid semiconductor devices, the ionogel offers mechanical adaptability, including stretchability, self-healing, and reconfigurability, making them ideal for soft robotics applications. Furthermore, the ionogel demonstrates autonomous decision-making capabilities, allowing a robotic arm to mimic the selective trapping behavior of the Venus flytrap. This work highlights the transformative potential of modulated ion distribution and transport in soft materials, bridging the gap between biological intelligence and artificial systems. Our findings pave the way for advancements in soft robotics, human-machine interfaces, and bioinspired artificial intelligence, where adaptable, energy-efficient sensing, learning, and memory functions are essential.

## Methods

### Materials

Oligo(ethylene glycol) methyl ether acrylate (OEGA, average Mn = 480), [2-(acryloyloxy)ethyl]trimethylammonium chloride (DMAEA-Q, 80% aqueous solution), 1-Ethyl-3-Methylimidazolium Bis(Trifluoromethylsulfonyl)Imide ($[EMIM]^+$ $[TFSI]^-$, purity~99%) and 2-hydroxy-2-methylpropiophenone (HMPP, purity ~ 98%) were purchased from Sigma-Aldrich Co. Methyl acrylate (MA, purity ~ 98.5%) Lithium bis(trifluoromethanesulfonyl)imide (LiTFSI, purity ~ 99%) and Benzyl acrylate (BzA, purity ~ 97%) were purchased from Aladdin Co. Acetone (purity ~ 99%) was bought from Sinopharm Chemical Reagent Co. Green and yellow dyes were purchased from fleurcouleur Co. Carbon paper (TGP-H-060) was purchased from Toray Co.

### Preparation of the CPB and NPB

For the preparation of NPB, the molar ratio of MA to OEGA was 1:1, and the ionic liquid $[EMIM]^+$ $[TFSI]^-$ accounts for 5 wt% of the total mass. The mass concentration of HMPP was 0.5 wt%. The mixed precursor solution was vortexed, degassed, and then poured into a glass mold for UV-photoinitiated polymerization. The NPB was obtained after irradiation with UV light (12 W) for 30 min.

For the preparation of CPB, the $[DMAEA\text{-}Q]^+$ $[TFSI]^-$ monomer was first prepared according to a previous report[24]. Briefly, DMAEA-Q (11.3 g) was weighed into a round-bottom flask, heated to 70 °C with magnetic stirring, and stirred for 10 min. An aqueous LiTFSI solution (16.1 g in 30 mL of deionized water) was then added. The mixture was stirred for 2 h at room temperature. The upper aqueous phase was then decanted and the oil phase was washed with deionized water to remove inorganic salts. Finally, the oil phase was evaporated at 60 °C for about 1.5 h to obtain a colorless viscous product ($[DMAEA\text{-}Q]^+$ $[TFSI]^-$ monomer). Afterward, the $[DMAEA\text{-}Q]^+$ $[TFSI]^-$ monomer was mixed with the BzA and OEGA monomers. The monomer ratio was varied to tune the IDL strength and rectification effect. The optimal molar ratio of $[DMAEA\text{-}Q]^+$ $[TFSI]^-$, BzA, and OEGA was 3.4:2:1. The concentrations of $[EMIM]^+$ $[TFSI]^-$ and HMPP were the same as those in NPB. Polymerization of the CPB was also performed under UV light irradiation (12 W) for 30 min. Unless otherwise noted, the length, width, and thickness of the tested CPB and NPB were 10, 10, and 1 mm, respectively. For photography, different food dyes were added to the precursor solution to indicate CPB (yellow color) and NPB (green color).

### Preparation of the bilayer ionogels

After separate preparation of the CPB and NPB ionogels, they were stored on silicone sheet substrates for later use. To fabricate the bilayer ionogels, free-standing CPB or NPB ionogels (unless otherwise specified, with dimensions of 10 × 10 × 1 mm) were carefully peeled off from the silicone substrates. The CPB/NPB bilayer structures were then assembled by directly attaching the bare surfaces of the two ionogels. To ensure sufficient contact between the two layers, the assembled bilayer ionogels were left to rest for 30 min before conducting any further testing. When the CPB and NPB layers come into contact, an IDL is naturally formed due to the migration of free anions and subsequent ion accumulation at the interface. This process generates electrostatic adhesion, and the resting period enhances the interfacial adhesion without requiring any additional treatments. For NPB/NPB or CPB/CPB bilayer structures, the inherent stickiness of the ionogels allows effective adhesion by simply bringing the surfaces into contact and leaving them undisturbed for 30 min.

### Fabrication of the bilayer ionogel array

Jelcon CH-8 conductive carbon paste was purchased from JuJo Chemicals Co. Ltd. and used to screen print the carbon electrodes onto a flexible silicone substrate[34]. The array consists of two layers of electrodes and sandwiched ionogels as shown in Supplementary Fig. 36. The electrodes were fabricated by screen printing the carbon paste. The screen (200 mesh) was made of polyester fabric and a coating layer of photosensitive adhesive (PLUS8000). The blade was made of polyurethane rubber with a Shore hardness of 85. The screen fabric was fixed to a flexible silicone substrate, then the carbon paste was applied to the screen fabric and quickly screen printed onto the substrate. A pressure of ~0.4 MPa was used when the blade was applied to produce the printed pattern. After drying at room temperature for 8 h, the printed electrodes were obtained. 9 pairs of bilayer ionogel were sandwiched between the screen-printed carbon electrodes, with CPB connected to the working electrode and NPB connected to the reference electrode.

### Characterizations and measurement

FTIR spectra were collected in the ATR mode on a Nicolet iS50 FTIR spectrometer. The rheological behavior of the bilayer ionogel was investigated on a Thermo Scientific HAAKE MARSTM 60 (modular advanced rheometer) instrument with a 25 mm parallel plate in an oscillation mode. To investigate the self-healing and reconfiguration capability of the ionogels, cyclic step-strain oscillatory tests from low-amplitude oscillations (0.1% strain) to high-amplitude oscillations (1000% strain) were performed at the frequency of 1 Hz and room temperature (25 °C). Tensile stress-strain curves were recorded on a universal testing machine (UTM2103, Shenzhen Suns Technology Co., Ltd.) at room temperature. The stretching rate was 50 mm $min^{-1}$.

ITC measurements were performed using an SV Nano instrument (TA Instrument, USA) to precisely analyze the titration process. The details of the experimental setup are as follows. Acetone was used as the solvent for both the BzA solution (80 mM) and the mixture ($[EMIM]^+$ $[TFSI]^-$ and $[DMAEA\text{-}Q]^+$ $[TFSI]^-$) solution, with the latter prepared in proportions identical to those in CPB. The calorimeter sample cell was thoroughly cleaned with acetone and rinsed with the prepared solution before the experiment. The titration began with an initial 4 µL injection of the BzA solution, followed by subsequent injections of 10 µL solution at 300-s intervals. The calibrated effective volume of the matrix solution cell was 950 µL. During the measurements, the solution in the sample cell was stirred continuously at 200 revolutions per minute to ensure uniform mixing. Heat signals were recorded starting 3 min before the first injection. All experiments were performed at 298 K.

All 180-degree peeling tests were conducted in ambient air at room temperature. The adhesion energy between different layers of the ionogels was measured using the 180-degree peeling tests. Polyester films were fixed to the ionogel samples as inextensible backing layers using cyanoacrylate glue. For sample preparation, CPB and NPB were cut to dimensions of 25 mm in length, 10 mm in width, and 1 mm in thickness. To ensure efficient interfacial adhesion, CPB and NPB were bonded together at their interface and left at room temperature for 2 h. Unless otherwise specified, the 180-degree peeling tests were performed on a mechanical testing machine (UTM2103, Shenzhen Suns) at a peeling speed of 100 mm $min^{-1}$. Once the peeling process reached a steady state, the measured peeling force plateaued. The adhesion energy was determined as two times the plateau value of the ratio of force to width. The interfacial toughness was calculated as $\Gamma = 2Fs/W$, where $Fs$ is the steady-state peeling force and $W$ is the width of the sample. To qualitatively analyze the influence of BzA and IDL on the interfacial adhesion, a DC power supply applied a DC voltage of +0.35/−1 V to each bilayer ionogel. In all of the asymmetric bilayer ionogels, the CPB was connected to the working electrode during the DC power application.

The voltage and current responses were recorded by electrochemical stations (CHI 760E). The open-circuit voltage ($V_{OC}$) of bilayer ionogels was recorded on a CHI 760E instrument. The resistance ($R$) of the ionogels was measured through electrochemical impedance spectroscopy (EIS) on a CHI 760E instrument. The conductivity ($\sigma$) was calculated based on the relationship of $\sigma = l/AR$, where $l$ is the length, and A is the cross-sectional area. Conductive carbon paper was used as the electrode. Unless otherwise specified, the thicknesses of the CPB and NPB were both 1 mm and the distance between the electrodes was 2 mm. The CPB was connected to the working electrode, while the NPB was connected to the reference electrode.

During the $I$–$V$ sweeping test, the sweep scan rate of the current vs. voltage ($I$–$V$) curves was 1 mV $s^{-1}$. The current density of the $I$–$V$ curves was calculated from the current divided by the original cross-sectional area of the ionogel device, which was 1 × 1 $cm^2$. Here the NPB was connected to the working electrode, while the CPB was connected to the reference electrode.

Alternating current impedance (AC impedance) were measured by electrochemical stations (CHI 760E) over a frequency range of 1000–0.1 Hz and an amplitude of 5 mV. Conductive carbon paper was used as the electrode. Unless otherwise specified, the cross-sectional area of the CPB/NPB, CPB/CPB, and NPB/NPB was fixed at 1 $cm^2$. The working electrode was connected to CPB. The reference electrode was connected to NPB for electrochemical measurements. The ZSimpWin software (version 3.60) was used to fit the experimental impedance data using equivalent circuits[18,19].

To evaluate the PPF behavior, the time interval ($\Delta t$) of the two consecutive current pulses and the amplitude of the current pulses were changed. The PPF index of the ionogels was defined as $A_2/A_1 \times 100\%$, where $A_1$ and $A_2$ are the amplitudes of the first and the second response voltage, respectively. To explore the multi-spiking effect of the bilayer ionogel, successive current pulses with an amplitude of 1 µA and different frequencies were applied. The energy consumption is calculated from the integration of the applied stimulus current and the response voltage over a time width. During the energy consumption test, the cross-sectional area of the ionogel device is varied. The $W$ is determined by $W = \int IdVdt$. For the memory evaluation, the training current was 10 µA (in the forward direction) and the real-time $V_{OC}$ was recorded immediately at the end of the training. To obtain a real-time display of an array's memory voltage on a smartphone screen, a Bluetooth module was connected to the array in Supplementary Fig. 37, allowing real-time transmission of the voltage signals to a smartphone.

### Statistics and reproducibility

All experiments (Fig. 2d–f) were repeated independently with similar results at least three times.

## Data availability

All data supporting the findings of this study are available within this article and the Supplementary Information or from the corresponding author upon request. The data generated in this study are provided in the Supplementary Information/Source Data file. Source data are provided with this paper.

## References


1. Yang, C. & Suo, Z. Hydrogel ionotronics. *Nat. Rev. Mater.* **3**, 125–142 (2018).
2. Robin, P. et al. Long-term memory and synapse-like dynamics in two-dimensional nanofluidic channels. *Science* **379**, 161–167 (2023).
3. Dobashi, Y. et al. Piezoionic mechanoreceptors: force-induced current generation in hydrogels. *Science* **376**, 502–507 (2022).
4. Xiao, K., Wan, C., Jiang, L., Chen, X. & Antonietti, M. Bioinspired ionic sensory systems: the successor of electronics. *Adv. Mater.* **32**, 2000218 (2020).
5. Keplinger, C. et al. Stretchable, transparent, ionic conductors. *Science* **341**, 984–987 (2013).
6. Jeong-Yun, S., Christoph, K., Whitesides, G. M. & Zhigang, S. Ionic skin. *Adv. Mater.* **26**, 7608–7614 (2014).
7. Lei, Z., Wang, Q., Sun, S., Zhu, W. & Wu, P. A bioinspired mineral hydrogel as a self-healable, mechanically adaptable ionic skin for highly sensitive pressure sensing. *Adv. Mater.* **29**, 1700321 (2017).
8. Lei, Z. & Wu, P. A highly transparent and ultra-stretchable conductor with stable conductivity during large deformation. *Nat. Commun.* **10**, 3429 (2019).
9. Lei, Z. & Wu, P. Bioinspired quasi-solid ionic conductors: materials, processing, and applications. *Acc. Mater. Res.* **2**, 1203–1214 (2021).
10. Kaspar, C., Ravoo, B. J., van der Wiel, W. G., Wegner, S. V. & Pernice, W. H. P. The rise of intelligent matter. *Nature* **594**, 345–355 (2021).
11. Lanza, M. et al. Memristive technologies for data storage, computation, encryption, and radio-frequency communication. *Science* **376**, eabj9979 (2022).
12. Luo, X. et al. A bionic self-driven retinomorphic eye with ionogel photosynaptic retina. *Nat. Commun.* **15**, 3086 (2024).
13. Wang, L., Zhang, P., Gao, Z. & Wen, D. Artificial tactile sensing neuron with tactile sensing ability based on a chitosan memristor. *Adv. Sci.* **11**, 2308610 (2024).
14. Xiong, T. et al. Neuromorphic functions with a polyelectrolyte-confined fluidic memristor. *Science* **379**, 156–161 (2023).
15. Zhao, S. et al. Programmable hydrogel ionic circuits for biologically matched electronic interfaces. *Adv. Mater.* **30**, 1800598 (2018).
16. Lei, Z. & Wu, P. Short-term plasticity, multimodal memory, and logical responses mimicked in stretchable hydrogels. *Matter* **6**, 429–444 (2023).
17. Ren, Y. et al. Ionic liquid–based click-ionogels. *Adv. Sci* **5**, eaax0648 (2019).
18. Kim, H. J., Chen, B., Suo, Z. & Hayward, R. C. Ionoelastomer junctions between polymer networks of fixed anions and cations. *Science* **367**, 773–776 (2020).
19. Jiang, F. et al. Ion rectification based on gel polymer electrolyte ionic diode. *Nat. Commun.* **13**, 6669 (2022).
20. Chen, W. et al. Cascade-heterogated biphasic gel iontronics for electronic-to-multi-ionic signal transmission. *Science* **382**, 559–565 (2023).
21. Wang, S. et al. An organic electrochemical transistor for multimodal sensing, memory and processing. *Nat. Electron.* **6**, 281–291 (2023).
22. Yu, C. et al. Hydrogels as dynamic memory with forgetting ability. *Proc. Natl. Acad. Sci. USA* **117**, 18962–18968 (2020).
23. Bartoli, S. & Roelens, S. Binding of acetylcholine and tetramethylammonium to a cyclophane receptor: anion's contribution to the cation–π interaction. *J. Am. Chem. Soc.* **124**, 8307–8315 (2002).
24. Qiu, W., Zhang, C. & Zhang, Q. Versatile copolymer for stretchable and self-healable liquid-free ionic conductive elastomers. *ACS Appl. Mater. Interfaces* **14**, 42578–42585 (2022).
25. Zhu, W., Wu, B., Lei, Z. & Wu, P. Piezoionic elastomers by phase and iinterface engineering for high-performance energy-harvesting ionotronics. *Adv. Mater.* **36**, 2313127 (2024).
26. Wang, Y. et al. Compliant and robust tissue-like hydrogels via ferric ion-induced of hierarchical structure. *Adv. Funct. Mater.* **33**, 2210224 (2023).
27. Bocharova, V. & Sokolov, A. P. Perspectives for polymer electrolytes: a view from fundamentals of ionic conductivity. *Macromolecules* **53**, 4141–4157 (2020).
28. Wang, R.-Y. et al. Superionic bifunctional polymer electrolytes for solid-state energy storage and conversion. *Adv. Mater.* **35**, 2203413 (2023).
29. Sun, T. L. et al. Bulk energy dissipation mechanism for the fracture of tough and self-healing hydrogels. *Macromolecules* **50**, 2923–2931 (2017).
30. Levine, D. J. et al. A low-voltage, high-force capacity electroadhesive clutch based on ionoelastomer heterojunctions. *Adv. Mater.* **35**, 2304455 (2023).
31. Sun, J.-Y. et al. Highly stretchable and tough hydrogels. *Nature* **489**, 133–136 (2012).
32. Lei, Z., Gao, W. & Wu, P. Double-network thermocells with extraordinary toughness and boosted power density for continuous heat harvesting. *Joule* **5**, 2211–2222 (2021).
33. Wu, Y. et al. Continuously tunable ion rectification and conductance in submicrochannels stemming from thermoresponsive polymer self-assembly. *Angew. Chem. Int. Ed.* **58**, 12481–12485 (2019).
34. Zhao, W., Lei, Z. & Wu, P. Mechanically adaptative and environmentally stable ionogels for energy harvest. *Adv. Sci.* **10**, 2300253 (2023).
35. Pan, Y., Pan, C., Mao, L. & Yu, P. Neuromodulation with chemicals: opportunities and challenges. *Fundam. Res.* https://doi.org/10.1016/j.fmre.2024.04.010 (2024).
36. Zhao, S. et al. Neuromorphic-computing-based adaptive learning using ion dynamics in flexible energy storage devices. *Natl. Sci. Rev.* **9**, nwac158 (2022).
37. van de Burgt, Y. et al. A non-volatile organic electrochemical device as a low-voltage artificial synapse for neuromorphic computing. *Nat. Mater.* **16**, 414–418 (2017).
38. Laughlin, S. B., de Ruyter van Steveninck, R. R. & Anderson, J. C. The metabolic cost of neural information. *Nat. Neurosci.* **1**, 36–41 (1998).
39. Zeng, H., Zhang, H., Ikkala, O. & Priimagi, A. Associative learning by classical conditioning in liquid crystal network actuators. *Matter* **2**, 194–206 (2020).
40. Jiang, C. et al. Mammalian-brain-inspired neuromorphic motion-cognition nerve achieves cross-modal perceptual enhancement. *Nat. Commun.* **14**, 1344 (2023).
41. Li, S. et al. Synaptic plasticity and learning behaviours mimicked through Ag interface movement in an Ag/conducting polymer/Ta memristive system. *J. Mater. Chem. C* **1**, 5292–5298 (2013).
42. Lou, D. et al. Double lock label based on thermosensitive polymer hydrogels for information camouflage and multilevel encryption. *Angew. Chem. Int. Ed.* **61**, e202117066 (2022).
43. Le, X. et al. A urease-containing fluorescent hydrogel for transient information storage. *Angew. Chem. Int. Ed.* **60**, 3640–3646 (2021).


## Acknowledgements

We gratefully acknowledge the financial support from the National Natural Science Foundation of China (Grant No. 22305033 received by Z.L., Grant No. 52433003 received by P.W.) and the Fundamental Research Funds for the Central Universities (2232024A-05 received by Z.L.).

## Author contributions

N.Z. carried out most experiments and co-wrote the manuscript. T.C. carried out the data processing in the supplementary text. Z.L. and P.W. supervised the project and co-wrote the manuscript. All authors discussed the results and revised the manuscript.

## Competing interests

The authors declare no competing interests.

## Additional information

**Supplementary information** The online version contains supplementary material available at https://doi.org/10.1038/s41467-025-59944-3.

**Correspondence** and requests for materials should be addressed to Zhouyue Lei or Peiyi Wu.

**Peer review information** *Nature Communications* thanks Anqiang Zhang and the other, anonymous, reviewer(s) for their contribution to the peer review of this work. A peer review file is available.